THE JOURNAL OF PHYSICAL CHEMISTRY C

ARTICLE

pubs.acs.org/JPCC

Surface Dangling Bond-Mediated Molecules Doping of Germanium Nanowires

Lin-bao Luo,*,† Xiao-bao Yang,‡ Feng-xia Liang,§ Jian-sheng Jie,*,† Chun-yan Wu,† Li Wang,† Yong-qiang Yu,† and Zhi-feng Zhu†

†School of Electronic Science and Applied Physics, Hefei University of Technology, Hefei, Anhui, 230009, P. R. China

‡Department of Physics, South China University of Technology, Guangzhou, 510641, Guangdong Province, P. R. China

§Department of Physics and Materials Science, City University of Hong Kong, Hong Kong SAR, P. R. China

Supporting Information

ABSTRACT: We report on the controllable doping of germanium nanowires (GeNWs) via selective molecule adsorption on the surface dangling bond. The GeNWs investigated are fabricated by evaporating pure germanium powder. Electron spin resonance analysis shows the presence of a surface dangling bond with g value of 2.023 and a spin density of C_{spin} = 2.47 × 10^{13} mg^{-1}. The as-prepared undoped GeNW exhibits typical p-type conduction behavior in air but n-type electrical characteristics in ammonia atmosphere. Significantly, the conductance, carrier mobility, and concentrations are found to be highly dependent on vacuum and ammonia gas pressures. Such an ambient effect could be explained by a surface dangling bond-mediated molecule doping model, according to which an acceptor or donor level is formed by water or ammonia adsorption, respectively. The generality of the above results suggests that surface dangling bond-mediated molecule doping may be applicable to modulation of the electrical characteristics of other semiconductor nanostructures.

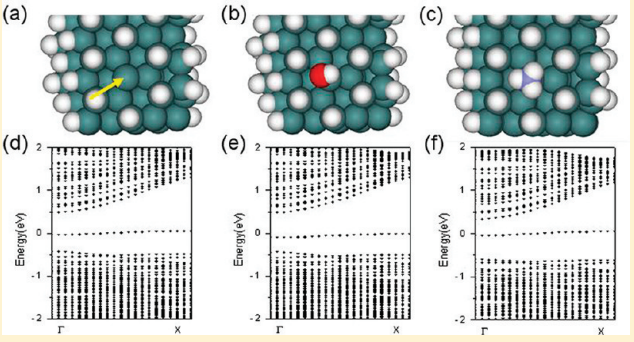

1. INTRODUCTION

Germanium, like silicon in group IV, is a very important material in semiconductor industry for its wide applications in fabricating various optoelectronic devices such as sensitive-light photodetector,[1,2] integrated circuits,[3] field effect transistor (FET),[4,5] lithium battery,[6,7] and high-efficiency photovoltaic cells.[8] One-dimensional germanium nanowires (GeNWs) have received special research interest lately due to their obvious superiority over silicon nanowires (SiNWs): (1) larger Bohr excitonic radius (24.3 nm for Ge vs 4.7 nm for Si), which allows a more prominent quantum confinement effect;[9] (2) higher electron and hole mobilities (μ_e =3900 $cm^2/(V\ s)$ and μ_h =1900 $cm^2/(V\ s)$ for Ge versus μ_e =1500 $cm^2/(V\ s)$ and μ_h =450 $cm^2/(V\ s)$ for Si);[10] and (3) predicted nanostructures with typical direct band gap characteristics.[11,12] To date, many progresses have been achieved in the synthesis of GeNWs; those includes electron beam lithography,[13,14] laser ablation,[15] physical or chemical vapor deposition,[16−18] oxide-assisted growth,[19] solution growth methods,[20−22] and so on.

Owing to the huge surface-to-volume ratio, the prominently different bonding characteristics and environment of the surface and interior make 1D semiconductor nanostructures de facto core−shell composites that typically have distinctly different properties from their bulk counterparts. Take SiNWs, for example. It has been reported that the surface species including impurity atoms termination, surface dangling bond, and adsorbents can signally influence their global fundamental properties (electrical, thermal, etc.).[23−25] This feature has been employed to not only develop chemical, gas, and biological sensors with exceptionally high sensitivity and good selectivity[26,27] but also to enable us to adjust the electrical property of the NWs by introducing different molecules on the their surfaces, which is completely different from the traditional volume-doping method by intentionally incorporating impurity atom into the bulk crystals. Despite these progresses in SiNWs, there is a sparsity of research activity dealing with the surface on GeNWs properties. As a result, the surface chemistry dependent electrical conduction property of GeNWs remains much less explored and understood thus far.[28,29] In this study, we present an investigation of ambient-dependent electrical conduction behavior of undoped but surface dangling bond-rich GeNWs by combination of both experimental characterization and theoretical simulation. The observed effective molecule doping will not only help provide a new alternative for modulation of semiconducting structures at nanoscale but also facilitate the development of new types of gas sensors with high sensitivity and good selectivity.

Received: September 9, 2011
Revised: October 24, 2011
Published: October 31, 2011

2. EXPERIMENTAL SECTION

Synthesis of the GeNWs. The synthesis setup used in this study is a high-temperature, three-zone tube furnace. To grow GeNWs, we placed 2 g of germanium powder (99.99%, purchased from Sigma-Aldrich Company) in an alumina boat at the zone 2. A piece of SiO_2 (500 nm)/p^+ Si wafer coated with a very thin layer of gold film was placed on zone 3, which is ~17 cm from the germanium source. After the tube was pumped down to a pressure of 1×10^{-2} mbar, high purity of mixed gas of H_2/Ar (5%/95%) was fed at a rate of 20 sccm. The zones 1 and 2 were then increased to 900 °C at a rate of 15 °C/min, and zone 3 was increased to 450 °C at a rate of 7.5 °C/min and kept for ~1 h. During the whole growth, the system was maintained at ~200 mbar. Finally, the products were collected from the SiO_2/Si substrate after the system was allowed to cool to nature temperature under the same gas flow and pressure.

Construction of the Single GeNW Field Effect Transistor. The collected substrate containing GeNWs was first immersed into a diluted HCl aqueous solution (0.1 M) for 30 s to remove germanium oxide formed during high-temperature growth. The GeNWs were then washed with distilled water and absolute alcohol, followed by transfer to an eppendorf to form dispersion. To construct the FET, we placed a drop of GeNW dispersion on SiO_2 (300 nm)/P^+ Si wafer to form a relatively uniform distribution of NWs on the substrate with desired density. Photolithography technique was utilized to define both source and drain electrodes. The gold electrodes were deposited by a high-vacuum (5×10^{-8} mbar) electron-beam evaporator.

Characterization of the GeNWs and Electrical Study of the GeNW-FET. The morphology, composition, and crystal structure of the product were investigated by scanning electron microscope (SEM, Philips XL 30 FEG), transmission electron microscope (TEM, Philips CM20, operating at 200 kV), high-resolution transmission electron microscope (HRTEM, Philips CM200 FEG, operating at 200 KV), and X-ray diffractometer (XRD, Siemens D-500). X-ray photoelectron spectroscopy (XPS) analysis was performed on a VG ESCALAB 3 spectrometer, using a monochromatic Al Kα source (1486.6 eV) at a base pressure of $<10^{-9}$ Torr. For ESR measurements, ~30 mg of GeNWs powder was filled in a standard ESR quartz sample tube. The ESR system (Bruker EMX-10/12) was operated at 9.75 GHz with modulation amplitude of 0.2 G and microwave modulation frequency of 100 kHz. For quantitative purpose, emery stone ($g = 2.005$) with a well-defined spin density of 10^{15} was employed as a standard reference. The evaluation of the GeNWs FET was carried out using a semiconductor $I-V$ system (CSC 4200, Keithley) with picoampere resolution.

Theoretical Simulation. We performed the density functional theory (DFT) calculations with the generalized gradient approximation (GGA) available in the VASP method. We set the energy cutoff at 420 eV and employed the PW91 exchange-correlation functional. The distance between GeNWs in neighboring supercells is 9 Å, which is large enough to eliminate cell-to-cell interaction. We adopted the Monkhorst-Pack sampling with a $1 \times 1 \times 4$ k-point grid for the optimization of GeNWs, which was $1 \times 1 \times 10$ for the band structures' calculation. For the GeNWs with DBs, we calculated a supercell containing 175 atoms (with a $1 \times 1 \times 1$ k-point grid) with the lattice of 17.08 Å along the axis direction, in which the DB interaction from different cells can be ignored. Using the conjugate gradient method, we fully optimized both the atomic configurations and the lattice constant of all models, with the force criteria set at 0.01 eV/Å.

3. RESULTS AND DISCUSSION

The GeNWs used were fabricated via conventional thermal evaporation of high-purity Ge powder. The fabrication setup is a three-temperature-zone tube furnace (cf. Figure 1a). After growth, the crystallinity of the products was briefly immersed into a diluted HF solution prior to XRD investigation. Figure 1b depicts the diffraction pattern acquired from the NWs, in which, all five peaks in the range from 20 to 80° can be readily indexed to diamond-like cubic phase Ge (JCPDF card no. 04-0545).[30]

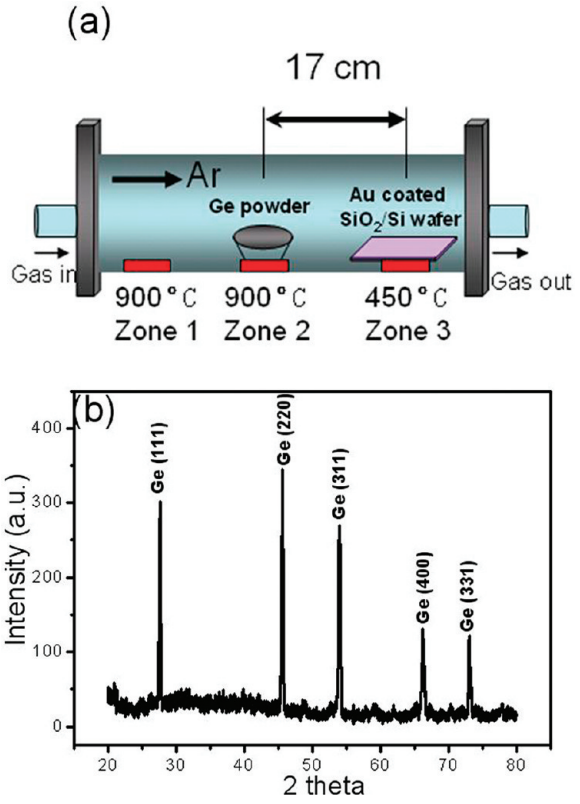

Figure 1. (a) Schematic illustration of the GeNWs synthesis setup. (b) XRD pattern of the as-collected GeNWs after brief immersion into diluted HF aqueous solution.

The SEM image in Figure 2a reveals high-yield growth of NWs material on the substrate. The GeNWs are up to tens of micrometers in length and exhibited high purity without any appreciable byproduct. Figure 2b shows a TEM image of a typical GeNW tipped with a gold nanoparticle (cf. SI-Figure 1 in the Supporting Information), whose presence suggests that during synthesis Au particles directed the 1D growth of GeNWs at high temperature via the widely accepted VLS mechanism.[31,32] Further selected area electron diffraction (SAED) combined with HRTEM study confirms the high-quality single-crystalline GeNWs grown by the thermal evaporation method. Careful examination of lattice fringes of more than 10 GeNWs indicates that the majority of the GeNWs have growth orientation along [110], whereas a fraction of GeNWs along [111], both of which have been observed on GeNWs synthesized via chemical vapor deposition approach.[33−36]

XPS experiment was performed to analyze the chemical composition on the NWs surfaces. As shown in the SI-Figure 2 in the Supporting Information, XPS survey spectrum is mainly composed of four typical peaks located at 30, 84, 285, and 532.5 eV due to Ge 3d, Au 4f, C 1s, and O 1s, respectively. The carbon peak attributable to surface adsorption is often observed in many other semiconductors nanostructures, and as usual, its

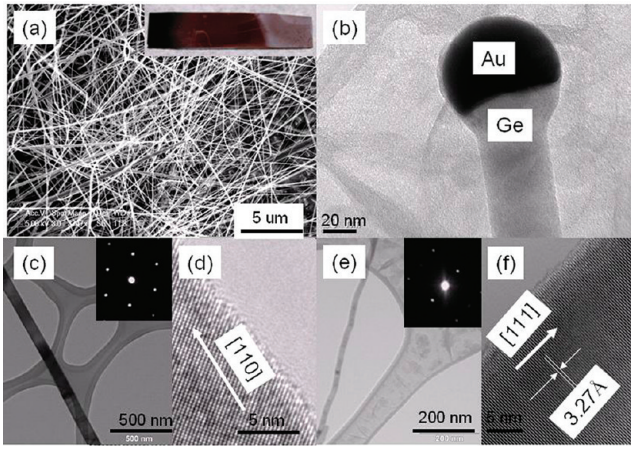

Figure 2. (a) SEM images of the GeNWs. Inset is a typical digital camera picture of the product. (b) TEM image of the GeNW with a gold nanoparticle on the head. (c) TEM image and selected area electron diffraction pattern (inset) of a typical GeNW with growth orientation along [110]. (d) HRTEM image of the GeNW shown in panel c. (e) TEM image and selected area electron diffraction pattern (inset) of a typical GeNW with growth orientation along [111]. (f) HRTEM image of the GeNW shown in panel e.

nominal influence can be left aside in the present study.[37] To get more information about the surface species, the Ge 3d peak was scanned individually. The XPS spectrum in Figure 3a shows the presence of germanium in the form of Ge, GeO, and GeO_2. The zerovalent Ge^0 is in the range from 29.2 to 30.2 eV, and Ge^{2+} and Ge^{4+} are in range from 31.2 to 32.6 eV. According to previous work, the Ge oxide and suboxide on GeNWs surface are formed at the sacrifice of Ge−H and Ge−Ge bonds, which has been verified by FTIR.[38]

Previously, Si oxide (including suboxide) and dangling bond have been observed on SiNWs that are prepared via oxide-assisted growth method.[39] To explore the possible presence of similar species on GeNWs, we carried electron spin resonance spectroscopy (ESR). Interestingly, the ESR spectrum as a function of external magnetic field in Figure 3b displays a distinct resonance at magnetic field of 3444.2 G with a line width of 40 G and g value of 2.023, suggesting the existence of unpaired orbits on the GeNWs surface. The g value is consistent with previous literature value of amorphous germanium and single crystal.[40,41] Because of limited relevant information available at present, it is impossible to figure out the precise structural configuration of such surface dangling bonds. However, the overall spin density could be determined to be $C_{spin} = 2.47 \times 10^{13}$ mg^{-1} from the ESR line by double integration of the experimental curve and comparison with emery stone.

To evaluate the electrical conduction property of the undoped GeNW in air, we measured the hole mobility and concentration of FET made from single GeNW. Figure 4a gives a schematic illustration of the device configuration, in which two parallel gold electrodes are bridged by an individual GeNW. The diameter of the NW is ~80 nm, and the effective gate length is 2.5 μm. Figure 4b shows the typical gate-dependent source-drain current versus source drain voltage curves at gate voltages from −40 to 0 V. Significantly, the conductance of the GeNW was found to increase (or decrease) with decreasing (or increasing) V_g, indicating typical p-type conduction characteristic. Figure 4c plots the typical transport characteristics of the GeNW-FET at

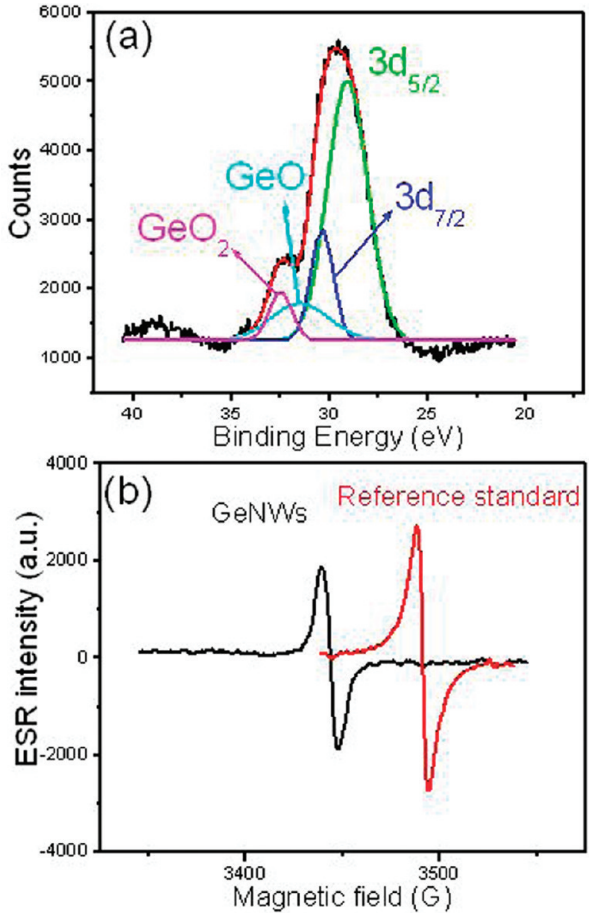

Figure 3. (a) XPS spectrum for Ge 3d peak. The labeled peaks are curve-fitting results, showing various surface chemical compositions. (b) ESR spectrum of GeNWs and standard reference at room temperature.

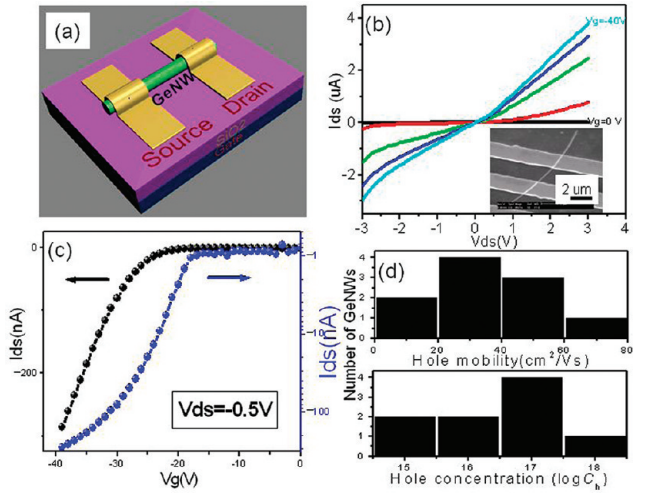

Figure 4. (a) Schematical illustration of the GeNW-FET. (b) I_{ds} versus V_{ds} curve under different V_g. Inset is the SEM image of a typical GeNW-FET. (c) I_{ds} versus V_g curve at $V_{ds} = -0.5$ V. (d) Statistical distribution of both hole mobility and concentration for 10 GeNWs.

a fixed V_{ds} of −0.5 V. By fitting the linear part of the I_{ds}-V_g curve, the turn-on threshold voltage (V_{th}) and transconductance (g_m),

dx.doi.org/10.1021/jp208708e |J. Phys. Chem. C 2011, 115, 24293–24299

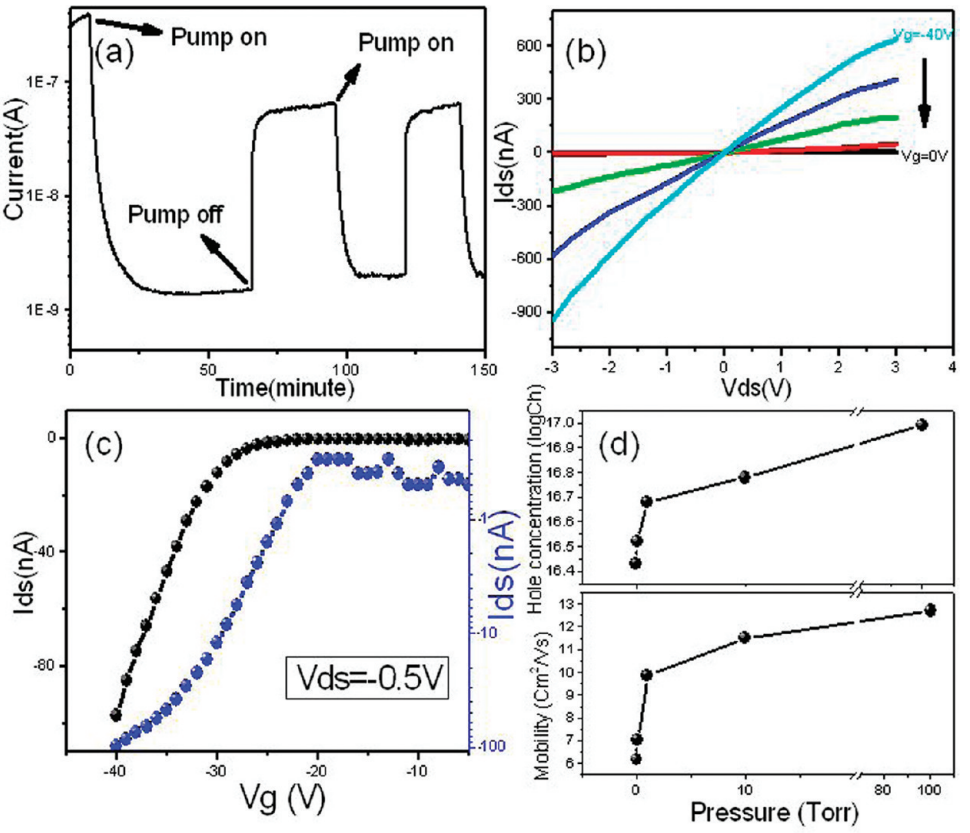

Figure 5. (a) Current variation of a typical GeNW in both air and vacuum; during measurement, V_{ds} is kept at 3 V. (b) In vacuum, I_{ds} versus V_{ds} curve under different V_g. (c) I_{ds} versus V_g curve at $V_{ds} = -0.5$ V. (d) Hole concentration and mobility at ambient pressures of 0.01, 0.1, 1, 10, and 100 Torr.

according to $g_m = dI_{ds}/dV_g$, are estimated to be 24.7 nS and −40 V, respectively. Hole mobility (μ_h) can be described by the formula of $\mu_h = g_m L^2/CV_{ds}$, where C is the NW capacitance and L is the effective GeNW length between electrodes. Assuming a cylinder on an infinite plate model for the GeNW-FET, the channel capacitance is determined by $C = 2\pi\varepsilon_0\varepsilon_{r,eff}L/\cosh^{-1}(t/r)$, where $\varepsilon_{r,eff}$ is the effective dielectric constant for SiO_2, t is the distance between p^+-Si substrate and the center of the GeNW, and r is the radius of the GeNW. On the basis of the above values, C and μ_h are calculated to be 2.01×10^{-16} F and 15.4 $cm^2/(V\,s)$, respectively. The resistivity of the GeNW is 3.01 Ω cm according to $\rho = R\pi r^2/L$; the hole concentration (n_h) is estimated to be 1.35×10^{17} cm^{-3} from the relation of $n_h = 1/\rho q\mu_h$. Hole mobility and concentration of 10 GeNWs were examined to evaluate systematically the electrical property of GeNWs from the same sample, as depicted in Figure 3d; it is visible that the majority of hole mobility for GeNW-FET lies in the range from 10 to 70 $cm^2/(V\,s)$, and hole concentration is in the range from 10^{15} to 10^{18} cm^{-3}. Understandably, this variation can be ascribed to the different surface state, which is resultant from diameter fluctuation.

As to the electrical property of intrinsic germanium bulk, it is well-established that electrical conduction can take place if electrons are generated by the addition of external energy in the form of light or heat, creating equal numbers of carriers. This will lead to weak n-type electrical characteristics because the electron mobility is approximately twice as great as that of hole. However, in this study, the conductivity of undoped GeNWs is dominated by holes, in consistence with the GeNWs obtained by a vapor−liquid−solid (VLS) method.[42] We attribute such a p-type behavior to the strong surface effect considering the

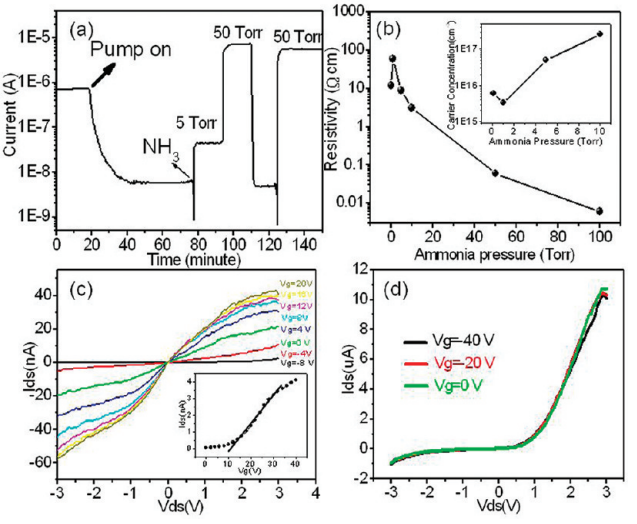

Figure 6. (a) Current variation of a typical GeNW in vacuum and upon NH_3 purging; during measurement, V_{ds} is kept at 3 V. (b) Resistivity at ammonia pressure of 0.1, 1, 5, 10, 50, 100 Torr. Inset is the carrier concentration at ammonia pressure of 0.1, 1, 5, 10 Torr. (c) I_{ds} versus V_{ds} curves at different gate voltages in ammonia gas with pressure of 5 Torr. Inset is the I_{ds} versus V_g curve, when $V_{ds} = 0.1$ V. (d) $I_{ds}-V_{ds}$ curves at different gate voltages in ammonia gas with pressure of 50 Torr.

following fact: (1) The GeNWs were prepared by means of evaporating pure Ge powder; this ensures that the GeNWs are all undoped. (2) Although gold nanoparticles were used as catalyst and some of the Au atoms in the junction area may inevitably diffuse into the GeNWs body during growth, the resultant defect level is too deep to contribute to the *p*-type conduction characteristic.[43]

Next, electrical property of GeNW at different ambient was compared with the unveiled ambient effect. Figure 5a plots the current evolution measured alternately in vacuum and in air. Apparently, the GeNW shows reversible switching between high and low conductance with a current ratio (I_{air}/I_{vac}) of about one to two order, when the ambient was switched from air to vacuum. Comparison of I_{ds}-V_g characteristics in air and in vacuum (0.01 Torr) found that the hole mobility decreases from 15.4 $cm^2/(V\,s)$ in air to 6.16 $cm^2/(V\,s)$ in vacuum. Meanwhile, hole concentration decreases from 1.35×10^{17} to 2.69×10^{16} cm^{-3}. Further study of six representative GeNWs confirms the high reproducibility of such an ambient effect (cf. SI-Figure 3 in the Supporting Information). Figure 5d shows the change in electrical property at different ambient pressure (0.01, 0.1, 1, 10, and 100 Torr). A gradual increase in both hole concentration and mobility is observed with increasing pressure. That is, the higher the pressure, the higher the hole concentration and mobility. In view of the tight relationship between water molecule and vacuum pressure, the notable ambient-dependent electrical property can be regarded as a consequence of water molecule adsorption. Theoretical explanation on how water molecule affects the GeNWs' electrical property will be entertained later on.

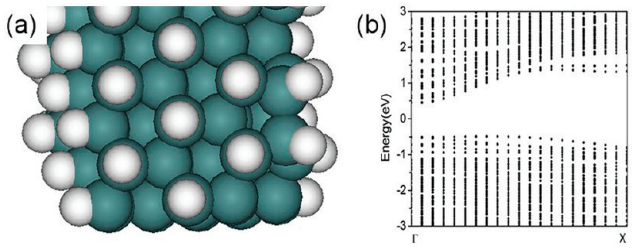

Figure 7. (a) Geometry of H-terminated GeNW. (b) Corresponding band structure.

The response of GeNW to NH_3 was also investigated. To eliminate the interference from water molecules, the chamber was first evacuated by rotary pump for ~60 min to allow the conductance to stabilize completely. It is interesting to observe that when the GeNW was exposed to NH_3 (5 Torr), the current suddenly slashed at first and then bounced sharply to $\sim 10^{-7}$ A, namely, in a V shape. In fact, this phenomenon is also echoed by the resistivity as a function of NH_3 pressure in Figure 6b. For cause analysis purpose, we studied the V_g-dependent V_{ds}-I_{ds} curve at 5 Torr. As shown in Figure 6c, remarkably, it demonstrates typical *n*-type electrical conduction behavior with electron mobility and concentration of 0.503 $cm^2/(V\,s)$ and 4.95×10^{16} cm^{-3}, respectively. Moreover, a similar ammonia pressure-dependent electrical property is also observed at pressures ranging from 1 to 10 Torr. Considering that the undoped GeNWs in vacuum exhibit typical *p*-type electrical conduction behavior, the aforementioned V-shape in current may be accountable with rapid carrier compensation.[44] As the pressure increased to 50 Torr, the current increased to $\sim 10^{-5}$ A accordingly. V_{ds}-I_{ds} curve at this pressure (Figure 6d) reveals that the contact between NW and gold electrode becomes nonlinear and asymmetric, probably as a result of the formation of Schottky contact. Besides, the gate voltage cannot modulate the source drain current, suggesting a very high concentration of electron generated at this pressure. These results definitely prove that the electron concentration can be effectively tuned by NH_3 pressure.

To elucidate the origin of the above molecule-induced doping effect, hydrogen-terminated GeNWs without any molecules adsorption and surface dangling bonds were first considered. As expected, it fails to induce an energy level within the band gap in the form of either acceptor level (*p*-type) or donor level

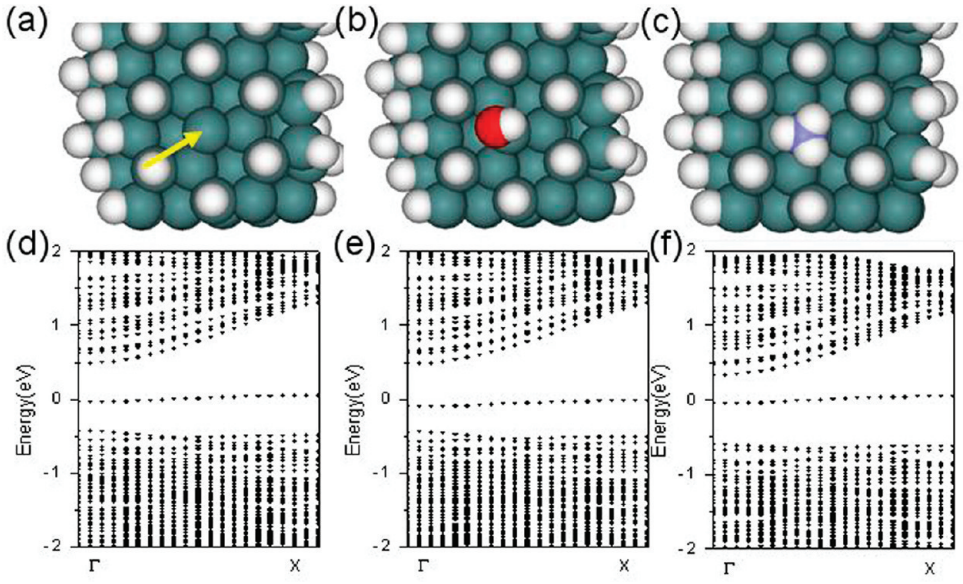

Figure 8. (a–c) Geometries of H-defect GeNW, H-defect GeNW with an adsorbed H_2O, and NH_3 molecule, respectively; the arrow in yellow color in panel a points to the position of the surface dangling bond. (d–f) Band structures for panels a–c, respectively. H-defect yields *p*-type doping. H_2O can enhance the *p*-type doping, whereas NH_3 yields *n*-type doping. Red and cornflower blue spheres denote O and N atom, respectively, whereas white and dark cyan spheres, respectively, represent H and Si atom.

(*n*-type), which is usually responsible for extrinsic electrical conduction (cf. Figure 7). This result explicitly excludes the possibility that the *p*-type electrical conduction of the GeNW in vacuum is due to hydrogen termination. On the basis of first-principles calculations, Rurali et al. lately reported that *n*-type and *p*-type doping of surface dangling bond-riched Si nanowire could be theoretically achieved by exposure to NH_3 and NO_2, respectively.[45] Enlightened by this, we propose that the selective molecule doping be attributed to the similar mediation role the surface dangling bond played at different ambient, given that silicon and germanium share many properties in common, and there is indeed a large quantity of surface dangling bond observed on the as-synthesized GeNW surface. To justify this hypothesis, we simulated at different ambient the defect level variation of the dangling bond-riched, [110]-oriented GeNW. The surface dangling bond was formed by removing one hydrogen atom from the H-terminated GeNW, which has been universally adopted in GeNW- and SiNW-related theoretical simulation.[46,47] Additionally, the GeNW under investigation was a typical [110] one with a rhombus cross-section enclosed by (111) facets. A collection of the geometry of dangling bond-riched GeNW at different ambient and their corresponding band structures are shown in Figure 8, from which it can be easily found that the defect level (E_d) without any molecule adsorption is 0.39 eV above the valence band maximum (VBM) and 0.43 eV (E_a) below the conduction band minimum (CBM). Interestingly, upon absorption of a water molecule, the E_d and E_a become 0.34 and 0.50 eV, revealing that the *p*-type conduction was enhanced, but when the absorbent was substituted with a NH_3 molecule, the defect level (E_d/E_a of 0.55/0.28 eV) moves to CBM to give rise to typical *n*-type electrical characteristics. These results are in good agreement with the foregoing experimental observation. It is worth noting that when water molecule adsorbs on surface dangling bond it is virtually a very weak interaction, and thus there is no chemical bond formed between Ge and O atoms, but when a NH_3 molecule is placed near the surface dangling bond, N−Ge bonding with energy of 0.5 eV (48.16 kJ/mol, similar to van der Waals force) was formed according to our theoretical calculation, yet the bonding is so weak that it is apt to break off with ease when NH_3 desorbs.

4. CONCLUSIONS

In summary, we have fabricated single-crystal GeNW on large scale by a general thermal evaporation approach. ESR analysis clearly shows the presence of surface dangling bond with *g* value of 2.023 and a spin density of $C_{spin} = 2.47 \times 10^{13}$ mg^{-1}. The as-prepared GeNW shows typical *p*-type conduction behavior in air but *n*-type electrical characteristics in ammonia atmosphere. Additionally, in both cases, the carrier concentration and mobility can be tuned by the gas pressures. Such surface molecule-dependent electrical characteristics can be satisfactorily interpreted by surface dangling bond-mediated molecule-doping model. The totality of the above results corroborates that appropriate molecule adsorption on the surface dangling bonds can allow effective doping, which is of significance to development of high-performance sensor and electronic devices.

■ ASSOCIATED CONTENT

Ⓢ Supporting Information. EDX spectrum of GeNWs, XPS survey spectrum of GeNWs, and comparison of hole mobility and concentration in vacuum and air. This material is available free of charge via the Internet at http://pubs.acs.org.

■ AUTHOR INFORMATION

Corresponding Author

*E-mail: luolb@hfut.edu.cn, jsjie@hfut.edu.cn.

■ ACKNOWLEDGMENT

This work was supported by the National Natural Science Foundation of China (nos. 60806028, 61106010, 21101051, 20901021, 1104080), the Program for New Century Excellent Talents in University of the Chinese Ministry of Education (NCET-08-0764), the Major Research Plan of the National Natural Science Foundation of China (no. 91027021), the Start-Up Fund of Hefei University of Technology, and the Fundamental Research Funds for the Central Universities (2011HGRJ0007, 2011ZM0090).

■ REFERENCES

(1) Polyakov, B.; Daly, B.; Prikulis, J.; Lisauskas, V.; Vengalis, B.; Morris, M. A.; Holmes, J. D.; Erts, D. *Adv. Mater.* **2006**, *18*, 1812–1816.
(2) Kim, C. J.; Lee, H. S.; Cho, Y. J.; Kang, K.; Jo, M. H. *Nano Lett.* **2010**, *10*, 2043–2048.
(3) Park, J. H.; Kapur, P.; Saraswat, K. C.; Peng, H. L. *Appl. Phys. Lett.* **2007**, *91*, 143107.
(4) Greytak, A. B.; Lauhon, L. J.; Gudiksen, M. S.; Lieber, C. M. *Appl. Phys. Lett.* **2004**, *84*, 4176–4178.
(5) Wang, D. W.; Wang, Q.; Javey, A.; Tu, R.; Dai, H. J.; Kim, H.; Mclntyre, P. C.; Krishnamohan, T.; Saraswat, K. C. *Appl. Phys. Lett.* **2003**, *12*, 2432–2434.
(6) Chan, C. K.; Candace, K.; Zhang, X. F.; Cui, Y. *Nano Lett.* **2008**, *8*, 307–309.
(7) Dileo, R. A.; Ganter, M. J.; Raffaelle, R. P.; Landi, B. J. *J. Mater. Res.* **2010**, *25*, 1441–1446.
(8) Ganguly, G.; Ikeda, T.; Nishimiya, T.; Saitoh, K.; Kondo, M.; Matsuda, A. *Appl. Phys. Lett.* **1996**, *69*, 4224–4226.
(9) Gu, G.; Burghard, M.; Kim, G. T.; Dusberg, G. S.; Chiu, P. W.; Krstic, V.; Roth, S. *J. Appl. Phys.* **2001**, *90*, 5747–5751.
(10) Nguyen, P.; Ng, H. T.; Meyyappan, M. *Adv. Mater.* **2005**, *17*, 549–553.
(11) Jing, M. W.; Ni, M.; Song, W.; Lu, J.; Gao, Z. X.; Lai, L.; Mei, W. N.; Yu, D. P.; Ye, H. Q.; Wang, L. *J. Phys. Chem. B.* **2006**, *110*, 18332–18337.
(12) Wu, X. Y.; Kulkarni, J. S.; Collins, G.; Petkov, N.; Almecija, D.; Boland, J. J.; Erts, D.; Holmes, J. D. *Chem. Mater.* **2008**, *20*, 5954–5967.
(13) Giovine, E.; Notargiacomo, A.; Di, G. L.; Palange, E.; Evangelisti, F.; Leoni, R.; Castellano, G.; Torrioli, G.; Foglietti, V. *Nanotechnology* **2001**, *12*, 132–135.
(14) Liu, J. L.; Lu, Y.; Shi, Y.; Gu, S. L.; Jiang, R. L.; Wang, F.; Bu, H. M.; Zheng, Y. D. *Phys. Status Solidi A* **1998**, *168*, 441–446.
(15) Morales, A.; Lieber, C. M. *Science* **1998**, *279*, 208–211.
(16) Kodambaka, S.; Tersoff, J.; Reuter, M. C.; Ross, F. M. *Science* **2007**, *316*, 729–732.
(17) Kamins, T. I.; Williams, R. S. *Nano Lett.* **2004**, *4*, 503–506.
(18) Li, C. B.; Usami, K.; Muraki, T.; Mizuta, H.; Oda, S. *Appl. Phys. Lett.* **2008**, *93*, 041917.
(19) Meng, X. M.; Hu, J. Q.; Jiang, Y.; Lee, C. S.; Lee, S. T. *Appl. Phys. Lett.* **2003**, *83*, 2241–2243.
(20) Fang, C.; Foll, H.; Carstensen, J. *Nano Lett.* **2006**, *6*, 1578–1580.
(21) Chockla, A. M.; Korgel, B. A. *J. Mater. Chem.* **2009**, *19*, 996–1001.
(22) Lin, L. W.; Tang, Y. H.; Chen, C. S.; Xu, H. F. *CrysEngComm* **2010**, *12*, 2975–2981.

(23) Luo, L. B.; Yang, X. B.; Liang, F. X.; Xu, H.; Zhao, Y.; Xie, X.; Zhang, W. F; Lee, S. T. *J. Phys. Chem. C.* **2011**, *115*, 18453–18458.
(24) Hochabum, A. I.; Chen, R. K.; Delgado, R. D.; Liang, W. J.; Gamett, E. C.; Najarian, M.; Majumdar, A.; Yang, P. D. *Nature* **2008**, *451*, 163–168.
(25) Jie, J. S.; Zhang, W. J.; Peng, K. Q.; Yuan, G. D.; Lee, C. S.; Lee, S. T. *Adv. Funct. Mater.* **2008**, *18*, 3251–3257.
(26) Kuang, Q.; Lao, C. S.; Wang, Z. L.; Xie, Z. X.; Zheng, L. S. *J. Am. Chem. Soc.* **2007**, *129*, 6070–6071.
(27) Luo, L. B.; Jie, J. S.; Zhang, W. F.; He, Z. B.; Wang, J. X.; Yuan, G. D.; Zhang, W. J.; Wu, L. C. M.; Lee, S. T. *Appl. Phys. Lett.* **2009**, *94*, 193101.
(28) Wang, D. W.; Tu, R.; Zhang, L.; Dai, H. *Angew. Chem., Int. Ed.* **2005**, *44*, 2925–2929.
(29) Wang, D. W.; Chang, Y. L.; Wang, Q.; Cao, J.; Darmer, D. B.; Gordon, R. G.; Dai, H. J. *J. Am. Chem. Soc.* **2004**, *126*, 11602–11611.
(30) Yan, C. Y.; Lee, P. S. *J. Phys. Chem. B* **2009**, *113*, 2208–2211.
(31) Das, K.; Chakraborty, A. K.; Nandagoswami, M. L.; Shingha, R. K.; Dhar, A.; Coleman, K. S.; Ray, S. K. *J. Appl. Phys.* **2007**, *101*, 074307.
(32) Li, L.; Fang, X. S.; Chew, H. G.; Zheng, F.; Liew, T. H.; Xu, X. J.; Zhang, Y. X.; Pan, S. S.; Li, G. H.; Zhang, L. D. *Adv. Funct. Mater.* **2008**, *18*, 1080–1088.
(33) Chockla, A. M.; Korgel, B. A. *J. Mater. Chem.* **2009**, *19*, 996–1001.
(34) Hanrath, T.; Korgel, B. A. *Small.* **2005**, *1*, 717–721.
(35) Gerung, H.; Boyle, T. J.; Tribby, L. J.; Bunge, S. D.; Brinker, C. J.; Han, S. M. *J. Am. Chem. Soc.* **2006**, *128*, 5244–5250.
(36) Chen, X. H.; Kim, M. H.; Zhang, X. Z.; Larson, C.; Yu, D. P.; Wodtke, A. M.; Moskovits, M. *J. Phys. Chem. C* **2008**, *112*, 13797–13800.
(37) Song, H. S.; Zhang, W. J.; Yuan, G. D.; He, Z. B.; Zhang, W. F.; Tang, Y. B.; Luo, L. B.; Lee, C. S.; Bello, I.; Lee, S. T. *Appl. Phys. Lett.* **2009**, *95*, 033117.
(38) Park, K. Y.; Lee, Y. W.; Lee, J. H.; Lim, S. W. *Appl. Surf. Sci.* **2008**, *254*, 4820–4828.
(39) Baumer, A.; Stutzmann, M.; Brandt, M. S.; Au, F. C. K.; Lee, S. T. *Appl. Phys. Lett.* **2004**, *85*, 943–945.
(40) Brodsky, M. H.; Title, R. S. *Phys. Rev. Lett.* **1969**, *23*, 581–585.
(41) Walters, G. K.; Estle, T. L. *J. Appl. Phys.* **1961**, *32*, 1854–1928.
(42) Zhang, S. X.; Hemesath, E. R.; Perea, D. E.; Wijaya, E.; Lensch-Falk, J. L.; Lauhon, L. J. *Nano Lett.* **2009**, *9*, 3268–3274.
(43) *Germanium-Based Technologies: From Materials To Devices*; Claeys, C., Simon, E., Eds.; Elsevier: London, 2007.
(44) Yuan, G. D.; Zhou, Y. B.; Guo, C. S.; Zhang, W. J.; Tang, Y. B.; Li, Y. Q.; Chen, Z. H.; He, Z. B.; Zhang, X. J.; Wang, P. F.; Bello, I.; Zhang, R. Q.; Lee, C. S.; Lee, S. T. *ACS Nano* **2010**, *4*, 3045–3052.
(45) Miranda-Duran, A.; Cartoixa, X.; Irisson, M. C.; Rurali, R. *Nano Lett.* **2010**, *10*, 3590–3595.
(46) Sankaran, K.; Pourtois, G.; Houssa, M.; Stesmans, A.; Caymax, M.; Heyns, M. M. *Appl. Phys. Lett.* **2009**, *94*, 184103.
(47) Lu, A. J.; Zhang, R. Q.; Lee, S. T. *Appl. Phys. Lett.* **2008**, *92*, 203109.